

Post-Quench Evolution of Distance and Uncertainty in a Topological System: Complexity, Entanglement, and Revivals

Tibra Ali,^(a) Arpan Bhattacharyya,^(b) S. Shajidul Haque,^(c) Eugene H. Kim,^(c) and Nathan Moynihan^(d)

^(a) *Perimeter Institute, 31 Caroline Street North, Waterloo, Ontario, Canada, N2L 2Y5*

^(b) *Center for Gravitational Physics, Yukawa Institute for Theoretical Physics, Kyoto University, Kitashirakawa Oiwakecho, Sakyo-ku, Kyoto 606-8502, Japan*

^(c) *Department of Physics, University of Windsor, Windsor, Ontario, Canada N9B 3P4*

^(d) *The Laboratory for Quantum Gravity & Strings, Department of Mathematics & Applied Mathematics, University Of Cape Town, Private Bag, Rondebosch, 7701, South Africa*

We investigate the evolution of the complexity and entanglement following a quench in a one-dimensional topological system, namely the Su-Schrieffer-Heeger model. We demonstrate that complexity can detect quantum phase transitions and shows signatures of revivals. This observation provides a practical advantage in information processing. We also show that the complexity saturates much faster than entanglement entropy; we elucidate the physics governing the evolution of these quantities, particularly the saturation timescale. Finally, we highlight a property to which the system's complexity is insensitive, but is captured by measures of entanglement, namely topological order.

In recent years, concepts from quantum information (QI) have helped to mold ideas in high-energy physics [1], namely anti de-Sitter/conformal field theory (AdS/CFT) duality [2], where a bulk AdS geometry is dual to a CFT living on the boundary. Recent progress has made evident that the entanglement of a (boundary) CFT is related to the emergence of the bulk geometry [3]. This relationship becomes even more puzzling in the context of black hole physics. In some black hole settings, entanglement is not sufficient to capture the dual geometric description. In some situations, certain bulk quantities continue to evolve even after the boundary CFT has equilibrated [4]. As a way out of this conundrum, Susskind proposed that the boundary quantity which continues to evolve after equilibration is the state's *complexity* [4, 5] and is dual to a volume of codimension-1 time-slice in the bulk AdS spacetime.

Central in QI are notions of *distance* and *uncertainty* [6]. Entanglement is quantified by measures of uncertainty and complexity is a measure of distance. Complexity is a concept from the theory of quantum computation [6, 7]. It is the shortest distance between some reference state $|\psi_R\rangle$ and a target state $|\psi_T\rangle$. Operationally, it quantifies the minimal number of operations needed to manipulate $|\psi_R\rangle$ to $|\psi_T\rangle$. Entanglement in quantum field theory has been well studied, and has led to a variety of insights [8, 9]. An understanding of complexity in quantum field theory is in its infancy – Refs. 10 considered circuit complexity in free bosonic quantum field theory using Nielsen's approach [11] (this has been generalized for interacting theories in [12]); Refs. 13 considered complexity for the same theory using the Fubini-Study distance; complexity for free fermionic theories was discussed in [14] and [15]; Refs. 16 defines complexity using path-integral; Refs. 17 and 18 discussed the complexity following a quench in bosonic theories. Furthermore, the time evolution of complexity for thermofield-double states has been studied in [19].

In this work, we investigate the time evolution of (measures of) distance and uncertainty following a quantum quench. We compare the evolution of the complexity

(for both the circuit complexity and Fubini-Study approaches) and fidelity with measures of entanglement. To begin with, we elucidate the physics governing the evolution of these quantities, and in particular, their saturation. In the black hole setting, complexity is expected to saturate later than the entanglement entropy. For the system considered here, the opposite occurs. This counterexample raises confusion regarding the holographic description of complexity. Secondly, we investigate revivals in the complexity. We also explore whether complexity can detect different phase transitions. Finally, we highlight a property to which the system's complexity is insensitive, but is captured by measures of entanglement, namely *topological order*. Our medium for these inves-

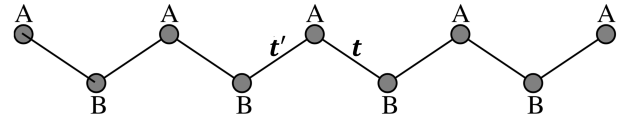


FIG. 1. The Su-Schrieffer-Heeger model – a one-dimensional system with A and B sublattices; electrons can tunnel between nearest-neighbor sites with intracell (intercell) tunneling amplitude t (t').

tigations is a one-dimensional topological insulator [20], namely the Su-Schrieffer-Heeger (SSH) model [21]. This is a tractable system exhibiting a nontrivial phase diagram, for which these ideas can be scrutinized in detail. It should be noted, so far complexity (and its comparison with entanglement) has only been explored in the context of simple toy models. This work takes steps toward bringing complexity closer to physical systems, and in particular, experiment. The SSH model was first introduced to understand the electronic properties of polyacetylene [21]. Recently, the SSH model has been realized experimentally in cold atom systems [22–25].

The SSH model is described by the Hamiltonian

$$\hat{H} = \sum_l \left[t \left(a_l^\dagger b_l + b_l^\dagger a_l \right) + t' \left(a_{l+1}^\dagger b_l + b_l^\dagger a_{l+1} \right) \right], \quad (1)$$

where a_l (b_l) destroys a fermion on site- l of sublattice- A (sublattice- B), and t (t') is the intracell (intercell) tunneling matrix element (see Fig. 1). The topological properties are determined by (t, t') . For $|t| < |t'|$ ($|t| > |t'|$), the system is a topological (topologically trivial) insulator; $|t| = |t'|$ is a quantum critical point (QCP), described by a $c = 1$ CFT. In what follows, we work in the Neveu-Schwarz sector. The system is readily analyzed in momentum space. By expanding the fermion operators in Fourier modes $[k = (2\pi/N)(m+1/2)]$ with $1 \leq m \leq N$

$$a_l = \frac{1}{\sqrt{N}} \sum_k e^{ikl} \tilde{a}_k \text{ and } b_l = \frac{1}{\sqrt{N}} \sum_k e^{ikl} \tilde{b}_k, \quad (2)$$

we get

$$\hat{H} = \sum_k (\tilde{a}_k^\dagger, \tilde{b}_k^\dagger) \begin{pmatrix} 0 & t + t' e^{-ik} \\ t + t' e^{ik} & 0 \end{pmatrix} \begin{pmatrix} \tilde{a}_k \\ \tilde{b}_k \end{pmatrix}. \quad (3a)$$

Eq. 3a is diagonalized by a Bogoliubov transformation [26]

$$\hat{H} = \sum_k E_k (\alpha_k^\dagger \alpha_k - \beta_k^\dagger \beta_k), \quad (3b)$$

where $E_k = \sqrt{t^2 + t'^2 + 2tt' \cos k}$. Physically, α_k (β_k) destroys a fermion of momentum- k in the conduction (valence) band.

We are interested in the quench dynamics of the SSH model –

$$\underline{t < 0} : \hat{H} = \hat{H}_<(t_<, t'_<) \quad , \quad \underline{t \geq 0} : \hat{H} = \hat{H}_>(t_>, t'_>). \quad (4)$$

In what follows, we take $|\psi_R\rangle$ to be the ground state of $\hat{H}_<$. We take $|\psi_T\rangle$ as the state obtained by evolution with $\hat{H}_>$: $|\psi_T\rangle = \exp(-it\hat{H}_>)|\psi_R\rangle$. More explicitly, let $\{\alpha_{<k}, \beta_{<k}\}$ denote the destruction operators of $\hat{H}_<$. The initial state has the valence band of $\hat{H}_<$ completely filled

$$|\psi_R\rangle = \prod_k \beta_{<k}^\dagger |0\rangle, \quad (5a)$$

where $|0\rangle$ is the Fock vacuum. The final state can be written as [26]

$$|\psi_T\rangle = \prod_k \frac{1}{\sqrt{1 + |z_k(t)|^2}} (\beta_{<k}^\dagger + z_k(t) \alpha_{<k}^\dagger) |0\rangle. \quad (5b)$$

We are interested in characterizing the circuit complexity for reaching the target state (Eq. 5b) from the reference state (Eq. 5a). A measure of circuit complexity is obtained from the *correlation matrix*, $\hat{C}_k(t)$, defined by

$$\hat{C}_k(t) = \langle \psi(t) | \Psi_k \Psi_k^\dagger | \psi(t) \rangle, \quad (6)$$

where $\Psi_k^T = (\tilde{a}_k, \tilde{b}_k)$ [26]. More specifically, we evolve the initial correlation matrix $\hat{C}_k(t=0)$ by the unitary operator $\tilde{U}_k(s)$ [15],

$$\tilde{C}_k(s) \equiv \tilde{U}_k(s) \hat{C}_k(t=0) \tilde{U}_k^\dagger(s), \quad (7)$$

with $\tilde{C}_k(s=1) = \hat{C}_k(t)$ and $\tilde{U}_k(s)$ is parameterized as the path-ordered exponential

$$\tilde{U}_k(s) = \mathcal{P} \exp \left[- \sum_I \int_0^1 ds Y_k^I(s) M_I \right], \quad (8)$$

where the $\{M_I\}$ are group generators, the $\{Y_k^I\}$ are control functions, and s parameterizes the path. Then, we define a “cost functional,” $\mathcal{C}[\{\tilde{U}_k(s)\}]$, on the space of unitaries via

$$\mathcal{C}[\{\tilde{U}_k(s)\}] = \int_0^1 ds \sqrt{\sum_k \sum_I |Y_k^I(s)|^2}. \quad (9)$$

By judicious choice of the $\{Y_k^I\}$, we determine the optimal path, i.e. the geodesic (with respect to the cost functional) on the space of unitaries. Then the complexity is simply the length of the geodesic [26].

We will be interested in comparing the results for the circuit complexity with those obtained from the Fubini-Study line element. To this end, the space of states, Eq. 5b, is given by a Riemannian structure [27]. We start with the Bures distance [28, 29]

$$D_{12}^2 = 2[1 - \mathcal{F}_{12}], \quad (10a)$$

where \mathcal{F}_{12} is the *fidelity*

$$\mathcal{F}_{12} = |\langle \psi_1 | \psi_2 \rangle|. \quad (10b)$$

Next, we consider two nearby states $|\psi(\{z_k\})\rangle$ and $|\psi(\{z_k + dz_k\})\rangle$ and obtain the Fubini-Study line element

$$ds^2 = \sum_k \frac{|dz_k|^2}{(1 + |z_k|^2)^2}, \quad (11)$$

where $ds^2 \equiv \lim_{|\psi_2\rangle \rightarrow |\psi_1\rangle} D_{12}^2$. One recognizes each term in Eq. 11 to be the line element for a two-sphere S^2 in the CP^1 representation – the state manifold is $S^2 \times S^2 \times \dots \times S^2$. We define a metric on the state manifold as [30]

$$s = \sqrt{\sum_k s_k^2}, \quad (12a)$$

where

$$s_k = \int_0^t dt' \frac{1}{1 + |z_k|^2} \left| \frac{dz_k}{dt'} \right| \quad (12b)$$

is a (natural) metric on S^2 . The complexity \mathcal{C} is the length of the geodesic connecting $|\psi_R\rangle$ and $|\psi_T\rangle$.

We now discuss our results; we consider the following quenches: (1) topological \leftrightarrow non-topological (2) non-topological \leftrightarrow critical (3) topological \leftrightarrow critical. Results are shown for the following sets of parameters: (1) topological – ($t=0.2, t'=1$) (2) non-topological – ($t=1, t'=0.2$) (3) critical – ($t=1, t'=1$). We begin by characterizing the quenches. To this end, we consider the system’s entanglement; in what follows, we will be interested in the entanglement of a spatial partition. For this, we first partition

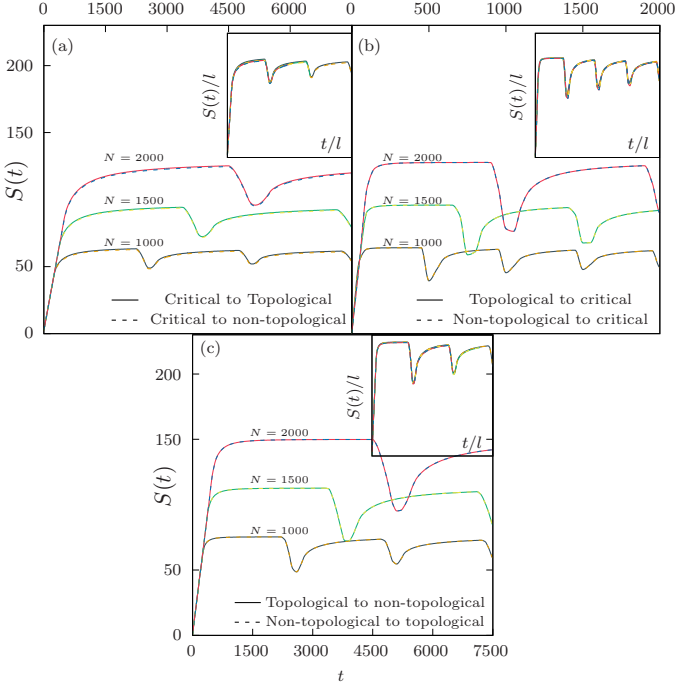


FIG. 2. Entanglement entropy as a function of time – results are shown for system sizes of $N=1000$, $N=1500$, $N=2000$ and entanglement partitions of length $l=100$, $l=150$, $l=200$, respectively. Quenching from (a) the critical point to a massive phase (b) a massive phase to the critical point (c) between massive phases. Insets: Entanglement entropy vs time scaled by the partition size, $S(t)/l$ vs t/l .

the system into two subsystems A and B and consider the correlation matrix restricted to subsystem- A , $\hat{C}^A(t)$, whose elements are ($m, n \in A$)

$$\hat{C}_{mn}^A(t) = \frac{1}{N} \sum_k \exp[ik(m-n)] \hat{C}_k(t). \quad (13)$$

We denote the eigenvalues of $\hat{C}^A(t)$ by $\{\lambda_n\}$, referred to as the entanglement spectrum (ES). Measures of entanglement are functions of this ES [26, 31, 32].

Fig. 2 shows results for the entanglement entropy (EE) [26]

$$S = - \sum [\lambda_n \ln \lambda_n + (1 - \lambda_n) \ln(1 - \lambda_n)]. \quad (14)$$

Results are shown for quenches from (a) the critical point to a massive phase (b) a massive phase to the critical point (c) between massive phases.

In all of the quenches, the EE first grows linearly and then saturates. At later times, one sees revivals due to the finite system size. Furthermore, we see that the amplitude is larger when quenching between massive phases (compared to when quenching to/from the critical point). The (pseudo-) period of the revivals is larger when quenching to a massive phase (compared to when quenching to the critical point). As shown in the insets, by working with scaled variables, namely S/l vs. t/l , the results collapse onto universal curves. While the results for the quenches have similar features, there are quantitative differences. In particular, when the initial phase

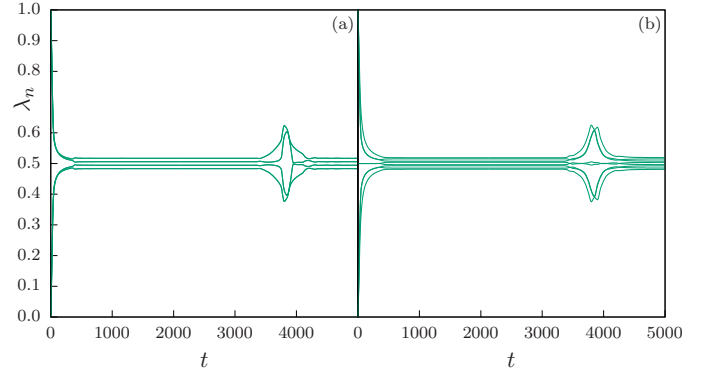


FIG. 3. Entanglement spectrum as a function of time – results are shown for a system size of $N=1500$ and an entanglement partition of $l=150$. Quenching from (a) the non-topological to the topological phase (b) the topological to the non-topological phase.

is the topological phase, the entropy is (a bit) larger, as the topological phase has greater entanglement.

To further characterize the properties of this system, ES is shown in Fig. 3. Fig. 3a (Fig. 3b) shows the ES for a quench from the non-topological (topological) to the topological (non-topological) phase. This shows very distinctly the differences in the quenches. In particular, the topological phase has “zero-modes” in the ES, namely states where $\lambda_n \simeq 1/2$. These are due to the edge states that are present in the topological phase (and absent otherwise) [32, 33]. When one starts initially in the topological phase, the zero-mode stays pinned [34]. [Results for the other quenches are qualitatively similar, namely quenches to/from the topological phase are clearly seen in the (evolution of the) zero-modes.]

We now discuss the system’s complexity. To get some intuition for how the complexity arises, Fig. 4 shows the

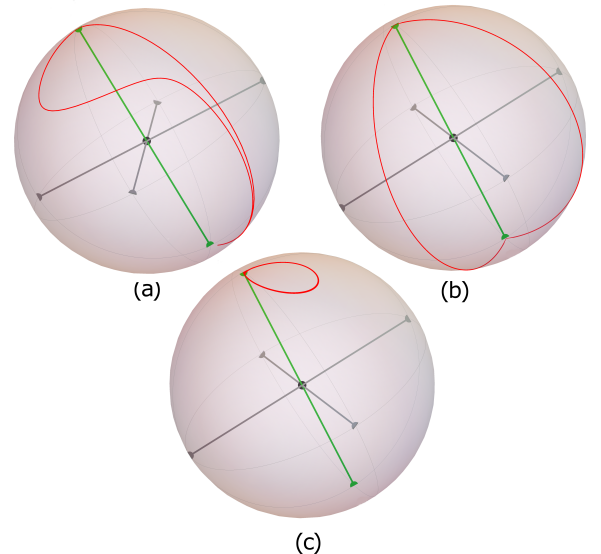


FIG. 4. Motion on the Bloch sphere upon quenching from the non-topological phase to the critical point: (a) $m = 470$ (b) $m = 505$ (c) $m = 870$. The system size is $N=1000$.

evolution of the target state upon quenching from the non-topological phase to the critical point for several values of k . As discussed above, Eq. 5b describes a trajectory on S^2 for each k . We see that Hamiltonian evolution gives rise to a variety of behaviors. Depending on the values of k , the evolution can be close to the geodesic for some values of k (Figs. 4a and b), while it can be rather distant for other values of k (Fig. 4c). Hence, for some values of k the path from Hamiltonian evolution gives the complexity, while for other values of k the contribution to the complexity comes from a very different path. [Similar results are obtained for the other quenches.]

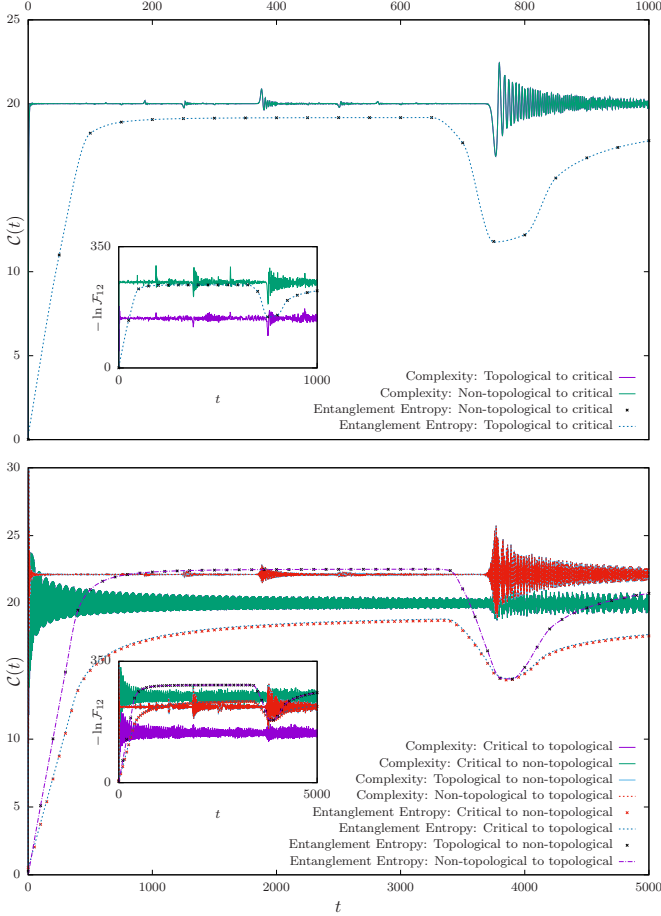


FIG. 5. The circuit complexity for a system of length $N=1500$. Quenching (a) from a massive phase to the critical point (b) to a massive phase. Insets: Negative logarithm of the fidelity: $-\ln \mathcal{F}_{12}$.

The evolution of the complexity is shown in Figs. 5 and 6. Figs. 5 shows results for the circuit complexity, while Figs. 6 shows results from the Fubini-Study line element. In both figures, panel (a) shows quenches from the massive phases to the critical point, while panel (b) shows quenches to a massive phase. For all the different quenches, the complexity grows extremely rapidly and then saturates, with some oscillations about the saturation value. When quenching to the critical point, distinct revivals appear in the complexity, similar to what occurs in the EE; when quenching to a massive phase, revivals also occur, but they are more pronounced when quenching between massive phases. To better understand these

results, the insets of Fig. 5 show results for the negative logarithm of the fidelity: $-\ln \mathcal{F}_{12}$. This quantity behaves similarly to the complexity. This gives insight into the behavior of the complexity and, in particular, its rapid growth and then saturation. This arises because the target state becomes orthogonal to the reference state rapidly. Note also that revivals appear in the fidelity when quenching to the critical point [35, 36]. However, we see that the signature in the complexity is more pronounced.

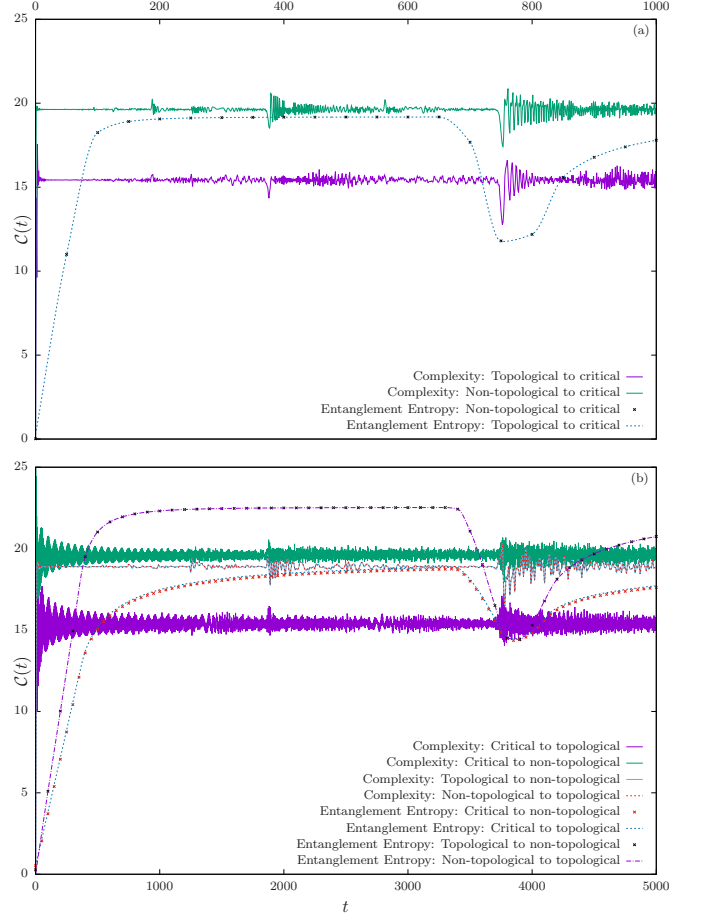


FIG. 6. The complexity from the Fubini-Study line element for a system of length $N=1500$. Quenching (a) from a massive phase to the critical point (b) to a massive phase.

Fig. 6 shows the complexity obtained from the Fubini-Study line element. This measure of complexity (like the fidelity) can clearly identify the different types of quenches. On the other hand, it appears the circuit complexity, just like entanglement entropy, can only distinguish quenches between the critical point and a massive phase from the quenches between the massive phases. It is not surprising that the circuit complexity and the entanglement entropy behave similarly, while the Fubini-Study approach and fidelity behave similarly. Both the circuit complexity and entanglement entropy are derived from the correlation matrix, while the Fubini-Study approach essentially follows from the fidelity. However, it is not immediately clear why the Fubini-Study approach provides a more sensitive measure of complexity than the circuit approach. In this work, we investigated the

evolution of distance and uncertainty following a quantum quench in a one-dimensional topological insulator, namely the Su-Schrieffer-Heeger model. For this model, the complexity saturated much more rapidly than the entanglement entropy. This is contrary to what happens in the blackhole scenario, where the complexity is expected to saturate exponentially slower than the entanglement entropy [5]. The mechanism for this rapid saturation of the complexity is tied to the rapid decay of the fidelity, namely because the final state becomes orthogonal to the initial state very rapidly. We suspect this quick saturation of the complexity is a generic feature to systems whose entanglement exhibit area-law scaling.

Another breakthrough was the observation of the revivals in the complexity. Note that the complexity is (much) less demanding computationally than the entanglement entropy, yet the complexity captures similar information such as revivals and information about different topological transitions. This makes the complexity rather appealing as a probe of quantum phase transitions.

Finally, we noted a potential drawback of complexity in systems with topological order. The topological order of the SSH model derives from the nontrivial topology of its Hilbert space [20]. Topological orders are readily probed on a manifold with a boundary. Gapless edge modes arise due to the topological order [33]. As an entanglement partition behaves as a physical boundary [37], gapless modes arise in topologically ordered systems, with support along the partition; the low-energy, universal part of the entanglement spectrum is due to these edge modes [38]. The complexity is a property of the

system's entire wave function [18]; as we saw, it does not give information about the topological order. Hence, the complexity appears to be a less sensitive probe than the entanglement (of a spatial partition).

Recently, it was demonstrated that, among the various approaches of computing complexity [10, 11, 13, 15], circuit complexity obtained directly from the wave function is the most effective [39]. Information is lost in approaches which do not characterize the complexity directly in terms of the system's wave function. It would be interesting to address this issue, doing a thorough comparison of the different approaches to complexity for fermionic systems (as was done for bosonic systems in [39]).

Acknowledgements: AB thanks Aninda Sinha, Pratik Nandy, Tadashi Takayanagi for useful discussions. AB is supported by JSPS Grant-in-Aid for JSPS fellowship (17F17023). EHK acknowledges support from funds from the University of Windsor. NM is supported by the South African Research Chairs Initiative of the Department of Science and Technology and the National Research Foundation (NRF) of South Africa; he was supported, in part, by the Perimeter Institute for Theoretical Physics during the course of this work. Research at Perimeter Institute is supported by the Government of Canada through the Department of Innovation, Science, and Economic Development, and by the Province of Ontario through the Ministry of Research and Innovation. Any opinion, finding and conclusion or recommendation expressed in this material is that of the authors and the NRF does not accept any liability in this regard.

-
- [1] M. Rangamani and T. Takayanagi, *Holographic Entanglement Entropy*, *Lect. Notes Phys.* **931** (2017) pp.1.
 - [2] J. M. Maldacena, *The large- N limit of superconformal field theories and supergravity*, *Adv. Theor. Math. Phys.* **2**, 231 (1998).
 - [3] See E. Bianchi and C. Rovelli (eds.), *Focus issue: entanglement and quantum gravity*, *Classical and Quantum Gravity* (Oct. 2014 - Mar. 2015).
 - [4] L. Susskind, *Computational complexity and black hole horizons*, *Fortsch. Phys.* **64**, 24 (2016).
 - [5] L. Susskind, *Entanglement is not enough*, *Fortsch. Phys.* **64**, 49 (2016).
 - [6] M. A. Nielsen and I. L. Chuang, *Quantum Computation and Quantum Information* (Cambridge University Press, New York, 2010).
 - [7] See e.g. S. Arora and B. Barak, *Computational Complexity: A Modern Approach* (Cambridge University Press, New York, 2009).
 - [8] See P. Calabrese, J. Cardy, and B. Doyon (eds.), *Special issue: entanglement entropy in extended quantum systems*, *J. Phys. A: Math. Gen.* **42**(50) (2009).
 - [9] L. Amico, R. Fazio, A. Osterloh, and V. Vedral, *Entanglement in many-body systems*, *Rev. Mod. Phys.* **80**, 517 (2008).
 - [10] R. A. Jefferson and R. C. Myers, *Circuit complexity in quantum field theory*, *JHEP* **10**, 107 (2017).
 - [11] M. A. Nielsen, M. R. Dowling, M. Gu, and A. C. Doherty, *Quantum Computation as Geometry*, *Science* **311**, 1133 (2006).
 - [12] A. Bhattacharyya, A. Shekar and A. Sinha, "Circuit complexity in interacting QFTs and RG flows," *JHEP* **1810** (2018) 140 [arXiv:1808.03105 [hep-th]].
 - [13] S. Chapman, M. P. Heller, H. Marrochio, and F. Pastawski, *Toward a definition of complexity for quantum field theory states*, *Phys. Rev. Lett.* **120**, 121602 (2018)
 - [14] R. Khan, C. Krishnan, and S. Sharma, *Circuit complexity in fermionic field theory*, arXiv:1801.07620.
 - [15] L. Hackl and R. C. Myers, "Circuit complexity for free fermions," *JHEP* **1807** (2018) 139 [arXiv:1803.10638 [hep-th]].
 - [16] P. Caputa, N. Kundu, M. Miyaji, T. Takayanagi and K. Watanabe, "Liouville Action as Path-Integral Complexity: From Continuous Tensor Networks to AdS/CFT," *JHEP* **1711** (2017) 097 [arXiv:1706.07056 [hep-th]].
A. Bhattacharyya, P. Caputa, S. R. Das, N. Kundu, M. Miyaji and T. Takayanagi, "Path-Integral Complexity for Perturbed CFTs," *JHEP* **1807** (2018) 086 [arXiv:1804.01999 [hep-th]].
 - [17] D. W. F. Alves and G. Camilo, *Evolution of complexity following a quantum quench in free field theory*, arXiv:1804.000107.
 - [18] H. A. Camargo, P. Caputa, D. Das, M. P. Heller, and R. Jefferson, *Complexity as a novel probe of quantum quenches: universal scalings and purification*

- arXiv:1807.07075 [hep-th].
- [19] S. Chapman, J. Eisert, L. Hackl, M. P. Heller, R. Jefferson, H. Marrochio and R. C. Myers, “Complexity and entanglement for thermofield double states,” arXiv:1810.05151 [hep-th].
- [20] For reviews, see M. Z. Hasan and C. L. Kane, *Colloquium: topological insulators*, Rev. Mod. Phys. **82**, 3045 (2010); X.-L. Qi and S.-C. Zhang, *Topological insulators and superconductors*, Rev. Mod. Phys. **83**, 1057 (2011).
- [21] W. P. Su, J. R. Schrieffer, and A. J. Heeger, *Solitons in polyacetylene*, Phys. Rev. Lett. **42**, 1698 (1979).
- [22] M. Atala, M. Aidelsburger, J. T. Barreiro, D. Abanin, T. Kitagawa, E. Demler, and I. Bloch, *Direct measurement of the Zak phase in topological Bloch bands*, Nat. Phys. **9**, 795 (2013).
- [23] M. Lohse, C. Schweizer, O. Zilberberg, M. Aidelsburger, and I. A. Bloch, *Thouless quantum pump with ultracold bosonic atoms in an optical superlattice*, Nat. Phys. **12**, 350 (2016).
- [24] S. Nakajima, T. Tomita, S. Taie, T. Ichinose, H. Ozawa, L. Wang, M. Troyer, and Y. Takahashi, *Topological Thouless pumping of ultracold fermions*, Nat. Phys. **12**, 296 (2016).
- [25] E. J. Meier, F. A. An, and B. Gadway, *Observation of the topological soliton state in the Su-Schrieffer-Heeger model*, Nat. Comm. **7**, 13986 (2016).
- [26] See the Appendix for details.
- [27] J. P. Provost and G. Vallee, *Riemannian structure on manifolds of quantum states*, Commun. Math. Phys. **76**, 289 (1980).
- [28] D. J. C. Bures, *An extension of Kakutani’s theorem on infinite product measures to the tensor product of semifinite w^* -algebras*, Trans. Amer. Math. Soc. **135**, 199 (1969).
- [29] A. Uhlmann, *The “transition probability” in the state space of a $*$ -algebra*, Rep. Math. Phys. **9**, 273 (1976).
- [30] See, e.g. M. Ó Searcoid, *Metric Spaces* (Springer, London 2007).
- [31] I. Peschel, *Calculation of reduced density matrices from correlation functions*, J. Phys. A: Math. Gen. **36**, L205 (2003).
- [32] E. H. Kim, *Characterizing topological order in superconductors via entanglement*, J. Phys.: Condens. Matter **26**, 205602 (2014).
- [33] X. G. Wen, *Quantum Field Theory of Many-body Systems* (Oxford University Press, New York, 2004).
- [34] M.-C. Chung, Y.-H. Jhu, P. Chen, C.-Y. Mou, and X. Wan, *A Memory of Majorana Modes through Quantum Quench*, Sci. Rep. **6**, 29172 (2016).
- [35] H. T. Quan, Z. Song, X. F. Liu, P. Zanardi, and C. P. Sun, *Decay of Loschmidt Echo Enhanced by Quantum Criticality*, Phys. Rev. Lett. **96**, 140604 (2006).
- [36] R. Jafari and H. Johannesson, *Loschmidt echo revivals: critical and non-critical*, Phys. Rev. Lett. **118**, 015701 (2017).
- [37] M. Srednicki, *Entropy and area*, Phys. Rev. Lett. **71**, 666 (1993).
- [38] H. Li and F. D. M. Haldane, *Entanglement spectrum as a generalization of entanglement entropy: identification of topological order in non-Abelian fractional quantum Hall effect states*, Phys. Rev. Lett. **101**, 010504 (2008).
- [39] T. Ali, A. Bhattacharyya, S. S. Haque, E. H. Kim, and N. Moynihan, *Time evolution of complexity: a critique of three methods* [arXiv:1810.02734 [hep-th]].

Appendix A: The System

We consider a fermionic Hamiltonian of the form

$$\hat{H}_F = \sum_k \Psi_k^\dagger \begin{pmatrix} \xi_k & \Delta_k \\ \Delta_k^* & -\xi_k \end{pmatrix} \Psi_k, \quad (\text{A1})$$

where Ψ_k is the spinor

$$\Psi_k^T = (\tilde{a}_k, \tilde{b}_k). \quad (\text{A2})$$

[For the SSH model, $\xi_k = 0$, $\Delta_k = t + t' \exp(-ik)$.] Eq. A1 is readily diagonalized

$$\hat{H}_F = \sum_k E_k \left(\alpha_k^\dagger \alpha_k - \beta_k^\dagger \beta_k \right), \quad (\text{A3})$$

where $E_k = \sqrt{\xi_k^2 + |\Delta_k|^2}$, and the $\{\alpha_k, \beta_k\}$ are related to the $\{\tilde{a}_k, \tilde{b}_k\}$ by the Bogoliubov transformation

$$\begin{pmatrix} \tilde{a}_k \\ \tilde{b}_k \end{pmatrix} = \begin{pmatrix} u_k & -v_k^* \\ v_k & u_k^* \end{pmatrix} \begin{pmatrix} \alpha_k \\ \beta_k \end{pmatrix}. \quad (\text{A4a})$$

In Eq. A4a,

$$u_k = \sqrt{\frac{1}{2} \left(1 + \frac{\xi_k}{E_k} \right)}, \quad v_k = \exp(-i\theta_k) \sqrt{\frac{1}{2} \left(1 - \frac{\xi_k}{E_k} \right)} \quad (\text{A4b})$$

with the phase defined via $\Delta_k = |\Delta_k| \exp(i\theta_k)$. Physically, α_k (β_k) destroys a fermion of momentum- k in the conduction (valence) band.

Appendix B: Quantum Quench

1. Quench Protocol

We consider a quench in the above model —

$$\underline{t < 0} : \hat{H} = \hat{H}_<(t_<, t'_<) \quad , \quad \underline{t > 0} : \hat{H} = \hat{H}_>(t_>, t'_>) . \quad (\text{B1a})$$

More explicitly, we consider

$$\underline{t < 0} : \hat{H}_< = \sum_k \Psi_k^\dagger \begin{pmatrix} \xi_k^< & \Delta_k^< \\ (\Delta_k^<)^* & -\xi_k^< \end{pmatrix} \Psi_k \quad ; \quad \underline{t > 0} : \hat{H}_> = \sum_k \Psi_k^\dagger \begin{pmatrix} \xi_k^> & \Delta_k^> \\ (\Delta_k^>)^* & -\xi_k^> \end{pmatrix} \Psi_k . \quad (\text{B1b})$$

Let $\{\alpha_{<k}, \beta_{<k}\}$ ($\{\alpha_{>k}, \beta_{>k}\}$) be eigenoperators of $\hat{H}_<$ ($\hat{H}_>$):

$$\begin{pmatrix} \tilde{a}_k \\ \tilde{b}_k \end{pmatrix} = \begin{pmatrix} u_{<k} & -v_{<k}^* \\ v_{<k} & u_{<k}^* \end{pmatrix} \begin{pmatrix} \alpha_{<k} \\ \beta_{<k} \end{pmatrix} \longrightarrow \hat{H}_< = \sum_k E_k^< \left(\alpha_{<k}^\dagger \alpha_{<k} - \beta_{<k}^\dagger \beta_{<k} \right) , \quad (\text{B2a})$$

$$\begin{pmatrix} \tilde{a}_k \\ \tilde{b}_k \end{pmatrix} = \begin{pmatrix} u_{>k} & -v_{>k}^* \\ v_{>k} & u_{>k}^* \end{pmatrix} \begin{pmatrix} \alpha_{>k} \\ \beta_{>k} \end{pmatrix} \longrightarrow \hat{H}_> = \sum_k E_k^> \left(\alpha_{>k}^\dagger \alpha_{>k} - \beta_{>k}^\dagger \beta_{>k} \right) . \quad (\text{B2b})$$

The $\{\alpha_{>k}, \beta_{>k}\}$ are related to the $\{\alpha_{<k}, \beta_{<k}\}$ by the unitary transformation

$$\begin{pmatrix} \alpha_{>k} \\ \beta_{>k} \end{pmatrix} = \begin{pmatrix} \mathcal{U}_k & -\mathcal{V}_k^* \\ \mathcal{V}_k & \mathcal{U}_k^* \end{pmatrix} \begin{pmatrix} \alpha_{<k} \\ \beta_{<k} \end{pmatrix} \quad (\text{B3a})$$

where

$$\mathcal{U}_k = u_{>k}^* u_{<k} + v_{>k}^* v_{<k} \quad , \quad \mathcal{V}_k = u_{>k}^* v_{<k} - v_{>k}^* u_{<k} . \quad (\text{B3b})$$

Then, $\hat{H}_>$ can be written in terms of the eigenoperators of $\hat{H}_<$ as

$$\hat{H}_> = \sum_k 2E_k^> \left[(|\mathcal{U}_k|^2 - |\mathcal{V}_k|^2) \tau_k^z - \mathcal{U}_k^* \mathcal{V}_k^* \tau_k^+ - \mathcal{U}_k \mathcal{V}_k \tau_k^- \right] , \quad (\text{B4})$$

where

$$\tau_k^- = \beta_{<k}^\dagger \alpha_{<k} , \quad \tau_k^+ = \alpha_{<k}^\dagger \beta_{<k} , \quad \tau_k^z = (\alpha_{<k}^\dagger \alpha_{<k} - \beta_{<k}^\dagger \beta_{<k})/2 \quad (\text{B5})$$

obey an $SU(2)$ algebra.

2. Reference and Target States

The time evolution operator can be written as

$$\hat{U}(t) = \prod_k \exp \left(\omega_k \tau_k^z + \alpha_k^+ \tau_k^+ + \alpha_k^- \tau_k^- \right) , \quad (\text{B6a})$$

where

$$\{\omega_k = -it2E_k^> (|\mathcal{U}_k|^2 - |\mathcal{V}_k|^2) , \quad \alpha_k^+ = it2E_k^> \mathcal{U}_k^* \mathcal{V}_k^* , \quad \alpha_k^- = it2E_k^> \mathcal{U}_k \mathcal{V}_k\} . \quad (\text{B6b})$$

In what follows, we take as our reference state, $|\psi_R\rangle$, the ground state of $\hat{H}_<$; we take as our target state, $|\psi_T\rangle$, the state obtained by evolution with $\hat{H}_>$: $|\psi_T\rangle = \exp(-it\hat{H}_>)|\psi_R\rangle$. The initial state has the valence band of $\hat{H}_<$ completely filled

$$|\psi_R\rangle = \prod_k \beta_{<k}^\dagger |0\rangle , \quad (\text{B7a})$$

where $|0\rangle$ is the Fock vacuum. The final state is given by

$$|\psi_T\rangle = \prod_k \frac{1}{\sqrt{1 + |z_k(t)|^2}} \left(\beta_{<k}^\dagger + z_k(t) \alpha_{<k}^\dagger \right) |0\rangle , \quad (\text{B7b})$$

where

$$z_k(t) = \frac{i2 \mathcal{U}_k^* \mathcal{V}_k^* \sin(E_k^> t)}{\cos(E_k^> t) + i(|\mathcal{U}_k|^2 - |\mathcal{V}_k|^2) \sin(E_k^> t)} . \quad (\text{B7c})$$

Note: To obtain Eqs. B7b and B7c, we utilized the decomposition [1]

$$\exp(\omega \tau^z + \alpha^+ \tau^+ + \alpha^- \tau^-) = \exp(\gamma_+ \tau^+) \exp[(\ln \gamma_0) \tau^z] \exp(\gamma_- \tau^-) , \quad (\text{B8a})$$

where

$$\gamma^0 = \left[\cosh \Omega - \frac{\omega}{2\Omega} \sinh \Omega \right]^{-2} , \quad \gamma^\pm = \left(\frac{\alpha^\pm}{2\Omega} \right) \frac{\sinh \Omega}{\cosh \Omega - (\omega/2\Omega) \sinh \Omega} , \quad (\text{B8b})$$

with

$$\Omega^2 = \omega^2/4 + \alpha^+ \alpha^- . \quad (\text{B8c})$$

[To simplify the notation, we have written γ^+ as z in Eq. B7b.]

Appendix C: State Manifold: Riemannian Metric; Geodesics and Complexity

The space of states obtained by evolution with Eq. B6a can be given a Riemannian structure [27]. Starting with the Bures distance

$$D_{12}^2 = 2[1 - \mathcal{F}_{12}]$$

where \mathcal{F}_{12} is the fidelity $\mathcal{F}_{12} = |\langle \psi_1 | \psi_2 \rangle|$. Then one considers two nearby states. Taylor expanding gives the line element [4]

$$ds^2 = \sum_{ij} g_{ij} dx^i dx^j , \quad (\text{C1a})$$

where $ds^2 \equiv \lim_{|\psi_2\rangle \rightarrow |\psi_1\rangle} D_{12}^2$, and we have introduced the metric tensor

$$g_{ij} = \text{Re} [\langle \partial_i \psi | \partial_j \psi \rangle] - \langle \partial_i \psi | \psi \rangle \langle \psi | \partial_j \psi \rangle . \quad (\text{C1b})$$

For states of the form Eq. B7b, the fidelity is given by

$$\mathcal{F}_{12} = \prod_k \frac{|1 + z_{1k}^* z_{2k}|}{\sqrt{1 + |z_{1k}|^2} \sqrt{1 + |z_{2k}|^2}} . \quad (\text{C2})$$

One obtains the line element

$$ds^2 = \sum_k \frac{|dz_k|^2}{(1 + |z_k|^2)^2} . \quad (\text{C3a})$$

$\forall k$ this is the line element for a two-sphere S^2 in the CP^1 representation. Writing $z_k = |z_k| \exp(i\phi_k)$ with $|z_k| = \tan \theta_k/2$, one obtains the line element in the spherical coordinates

$$ds^2 = \sum_k \frac{1}{4} (d\theta_k^2 + \sin^2 \theta_k d\phi_k^2) . \quad (\text{C3b})$$

This result (Eqs. C3a and C3b) is already anticipated by Eq. B6a – the time-evolution operator moves the system on the group manifold; $\forall k$, Eq. B6a moves the system on the Bloch sphere.

For a particular momentum, k , the arc-length between two points, s_k , is

$$s_k = \int_0^t dt' \frac{1}{1 + |z_k|^2} \left| \frac{dz_k}{dt'} \right| . \quad (\text{C4})$$

The geodesics are great circles; the arc-length of the geodesic, \mathcal{C}_k , is

$$\mathcal{C}_k = \frac{1}{2} \arccos [\cos \theta_1 \cos \theta_2 + \sin \theta_1 \sin \theta_2 \cos(\phi_1 - \phi_2)] , \quad (\text{C5a})$$

where (θ_1, ϕ_1) ((θ_2, ϕ_2)) are the spherical coordinates of the initial (final) point. [The prefactor of $1/2$ is the radius of the sphere.] As the initial state is given by Eq. B7a, one obtains $(|z_k| = \tan \theta_k/2)$

$$\mathcal{C}_k = \arctan |z_k| . \quad (\text{C5b})$$

For the full state manifold, $S^2 \times S^2 \times \dots \times S^2$, define a metric, s , as [5]

$$s = \sqrt{\sum_k s_k^2} . \quad (\text{C6})$$

It follows the system's complexity, \mathcal{C} , is

$$\mathcal{C} = \sqrt{\sum_k \mathcal{C}_k^2} . \quad (\text{C7})$$

Appendix D: Complexity and Entanglement from the Correlation Matrix

Define the *correlation matrix* \hat{C}_k [2, 3] –

$$\hat{C}_k(t) = \langle \psi(t) | \Psi_k \Psi_k^\dagger | \psi(t) \rangle , \quad (\text{D1})$$

where $\Psi_k^T = (\tilde{a}_k, \tilde{b}_k)$. Explicitly, one obtains

$$\hat{C}_k(t) = \begin{pmatrix} |u_k(t)|^2 & u_k(t)v_k^*(t) \\ v_k(t)u_k^*(t) & |v_k(t)|^2 \end{pmatrix} , \quad (\text{D2})$$

where

$$\begin{pmatrix} u_k(t) \\ v_k(t) \end{pmatrix} = \exp(-itH_>) \begin{pmatrix} u_{<k} \\ v_{<k} \end{pmatrix} \quad \text{with} \quad H_> = \begin{pmatrix} \xi_k^> & \Delta_k^> \\ (\Delta_k^>)^* & -\xi_k^> \end{pmatrix} . \quad (\text{D3})$$

From $\hat{C}_k(t)$, one obtains the complexity and measures of entanglement.

1. Complexity

We consider evolving the initial correlation matrix \hat{C}_k by the unitary operator \tilde{U}_k ,

$$\tilde{C}_k(s) \equiv \tilde{U}_k(s) \hat{C}_k(t=0) \tilde{U}_k^\dagger(s) , \quad (\text{D4})$$

with the boundary condition $\tilde{C}_k(s=1) = \hat{C}_k(t)$ i.e. at $s=1$ we recover the final correlation matrix. We parameterize \tilde{U}_k as the path-ordered exponential

$$\tilde{U}_k(s) = \mathcal{P} \exp \left[- \sum_I \int_0^1 ds Y_k^I(s) M_I \right] , \quad (\text{D5})$$

where the $\{M_I\}$ are group generators, the $\{Y_k^I\}$ are control functions, and s parameterizes the path; we define a “cost functional” on the space of unitaries $\mathcal{C}[\{\tilde{U}_k\}]$ via

$$\mathcal{C}[\{\tilde{U}_k\}] = \int_0^1 ds \sqrt{\sum_k \sum_I |Y_k^I(s)|^2} . \quad (\text{D6})$$

By judicious choice of the control functions $\{Y_k^I\}$, our goal is to determine the optimal path, namely the geodesic (with respect to the cost functional), on the space of unitaries; the complexity is the arc-length of the geodesic.

Taking the $\{M_I\}$ to be generators of $\text{SU}(2)$, \tilde{U}_k is readily parametrized as

$$\tilde{U}_k(s) = \begin{pmatrix} \cos \rho_k(s) \exp[i\phi_k(s)] & -i \sin \rho_k(s) \exp[-i\chi_k(s)] \\ -i \sin \rho_k(s) \exp[i\chi_k(s)] & \cos \rho_k(s) \exp[-i\phi_k(s)] \end{pmatrix} . \quad (\text{D7})$$

From Eq. D6, one obtains the (right-invariant) metric

$$ds^2 = \sum_k [d\rho_k^2 + \cos^2(\rho_k)d\phi_k^2 + \sin^2(\rho_k)d\chi_k^2]. \quad (\text{D8})$$

We solve for the geodesic with the boundary conditions

$$\rho_k(s=0) = 0, \quad \beta_k(s=0) = \chi_k^0 \quad (\text{D9a})$$

$$\rho_k(s=1) = \frac{1}{2} \arccos [\hat{C}_k(t)_{22} - \hat{C}_k(t)_{11}], \quad \beta_k(s=1) = \arctan \left[-\frac{\text{Re}\hat{C}_k(t)_{12}}{\text{Im}\hat{C}_k(t)_{12}} \right], \quad (\text{D9b})$$

where $\beta_k = \phi_k - \chi_k$. In the above equation(s), χ_k^0 is arbitrary. It is evident that we can either solve ϕ_k or χ_k unambiguously but not both of them. The subscripts (11,22,12) denote the components of \hat{C}_k . The simplest solution for the geodesic is,

$$\rho_k(s) = \rho_k(s=1)s, \quad \chi_k(s) = \chi_k^0, \quad \phi_k(s) = 0. \quad (\text{D10})$$

Then the complexity is given by

$$\mathcal{C}[\{\tilde{U}_k\}] = \frac{1}{2} \sqrt{\sum_k (\arccos [\sin^2(E_k^>t) \cos(2\theta_k^> - 2\theta_k^<) + \cos^2(E_k^>t)])^2}. \quad (\text{D11})$$

2. Entanglement

We are interested in the entanglement of a spatial partition. We partition the system into subsystems A and B . Measures of entanglement are obtained from the reduced density matrix for subsystem- A , $\hat{\rho}_A = \text{Tr}[\hat{\rho}]$ with $\hat{\rho}$ being the density matrix of the entire system. For the system considered in this work, $\hat{\rho}_A$ has the form [31, 32]

$$\hat{\rho}_A = \frac{1}{\mathcal{Z}} \exp(-\mathcal{H}_A) \quad (\text{D12a})$$

where

$$\mathcal{H}_A = \sum_{m,n \in A} \Psi_m^\dagger H_{mn}^A \Psi_n, \quad (\text{D12b})$$

and $\Psi_m^T = (a_m, b_m)$ is the spinor at site- m . Measures of entanglement are readily obtained from the correlation matrix restricted to subsystem- A [31, 32] – its elements are given by $(m, n \in A)$

$$C_{mn}(t) = \langle \psi(t) | \Psi_m \Psi_n^\dagger | \psi(t) \rangle. \quad (\text{D13})$$

$\hat{C}_{mn}(t)$ can be obtained from $\hat{C}_k(t)$ via

$$\hat{C}_{mn}(t) = \frac{1}{N} \sum_k \exp[ik(m-n)] \hat{C}_k(t). \quad (\text{D14})$$

Then, denoting the eigenvalues of $\hat{\mathbf{C}}$ by $\{\lambda_n\}$ ($0 \leq \lambda_n \leq 1$), the spectrum of H^A , $\{E_n\}$, is obtained via

$$E_n = \ln[(1 - \lambda_n)/\lambda_n]. \quad (\text{D15})$$

A central measure of entanglement is the Renyi entropy

$$S_\alpha = \frac{1}{1-\alpha} \ln \text{Tr}[\hat{\rho}_A^\alpha]. \quad (\text{D16a})$$

Explicitly,

$$S_\alpha = \frac{1}{1-\alpha} \sum_n \left[\ln(1 + e^{-\alpha E_n}) - \ln(1 + e^{-E_n})^\alpha \right]; \quad (\text{D16b})$$

using Eq. D15,

$$S_\alpha = \frac{1}{1-\alpha} \sum_n \ln[\lambda_n^\alpha + (1 - \lambda_n)^\alpha]. \quad (\text{D16c})$$

Taking $\alpha \rightarrow 1^+$ gives the entanglement entropy

$$S = - \sum [\lambda_n \ln \lambda_n + (1 - \lambda_n) \ln(1 - \lambda_n)] . \quad (\text{D17})$$

-
- [1] A. M. Perelomov, *Generalized Coherent States and Their Applications* (Springer-Verlag, Berlin, Heidelberg, 1986).
 - [2] I. Peschel, *Calculation of reduced density matrices from correlation functions*, J. Phys. A: Math. Gen. **36**, L205 (2003).
 - [3] E. H. Kim, *Characterizing topological order in superconductors via entanglement*, J. Phys.: Condens. Matter **26**, 205602 (2014).
 - [4] J. P. Provost and G. Vallee, *Riemannian structure on manifolds of quantum states*, Commun. Math. Phys. **76**, 289 (1980).
 - [5] See, e.g. M. Ó Searcóid, *Metric Spaces* (Springer, London 2007).
-